JOURNAL OF NEUROPHYSIOLOGY
Vol. 51, No. 1, January 1984. *Printed in U.S.A.*

Model of Electroretinogram b-Wave Generation: a Test of the K^+ Hypothesis

ERIC A. NEWMAN AND LOUIS L. ODETTE

Eye Research Institute of Retina Foundation, Boston 02114, and College of Engineering, Boston University, Boston, Massachusetts 02215

SUMMARY AND CONCLUSION

1. Generation of the electroretinogram b-wave is simulated with a computer model representing a dark-adapted amphibian retina. The simulation tests the K^+ hypothesis of b-wave generation, which holds that b-wave currents arise from localized Müller cell depolarizations generated by light-evoked increases in extracellular K^+ concentration, $[K^+]_o$.

2. The model incorporates the following components and processes quantitatively: *1*) two time-dependent K^+ sources representing the light-evoked $[K^+]_o$ increases in the inner and outer plexiform layers, *2*) a time- and $[K^+]_o$-dependent K^+ sink representing the $[K^+]_o$ decrease in the rod inner segment layer, *3*) diffusion of released K^+ through extracellular space, *4*) active K^+ reuptake and passive K^+ drift across the Müller cell membrane, *5*) spatial variations in the tortuosity factor and the volume fraction of extracellular space, *6*) an extraretinal shunt resistance. Müller cells are modeled with *1*) cytoplasmic resistance, *2*) spatial variations in membrane permeability to K^+, and *3*) a membrane potential specified by the Nernst equation and transmembrane current flow.

3. For specified K^+ source and sink densities, the model computes $[K^+]_o$ variations in time and retinal depth. Based on these $[K^+]_o$ distributions, Müller cell potentials, current source-density profiles, and intraretinal and transretinal voltages are calculated.

4. Imposed $[K^+]_o$ distributions similar to those seen experimentally during the b-wave lead to the generation of a transient b-wave response and to a prolonged Müller response in the model system. These response time courses arise because the b-wave is dominated by the short-lived distal $[K^+]_o$ increase, while the Müller response primarily reflects the long-lived proximal $[K^+]_o$ increase.

5. Current source-density distributions and intraretinal voltage profiles that are generated by the model at the peak of the b-wave closely resemble experimental results.

6. The model generates a realistic slow PIII potential in response to prolonged $[K^+]_o$ decreases in the distal retina and reproduces the K^+ ejection results of Yanagida and Tomita (50) accurately. Simulations also suggest that tissue damage caused by K^+-selective micropipettes in experimental preparations can lead to an underestimation of the distal $[K^+]_o$ increase.

7. The simulations demonstrate that the spatiotemporal properties of intraretinal b-wave voltages and currents and Müller cell responses can be generated according to the K^+ hypothesis: by passive Müller cell depolarization driven by variations in $[K^+]_o$.

INTRODUCTION

Glia are believed to contribute to the generation of extracellular field potentials in the central nervous system (6, 8, 22). Glial contributions to these potentials presumably arise from cell depolarization initiated by changes in extracellular K^+ concentration, $[K^+]_o$ (22). One of the best studied of these field potentials is the electroretinogram (ERG), a complex light-evoked potential generated by the retina. It has been suggested that several components of the ERG, including the prominent b-wave response, are generated by the major glial element of the retina, the Müller cell (12, 17, 26, 29, 41).

Faber (12) and Miller and Dowling (26) first suggested that the b-wave is generated by an interaction between extracellular K^+ increases and Müller cells in the retina. This "K^+ hypothesis" holds that increases in $[K^+]_o$ generated by neuronal activity locally depolarizes the Müller cell membrane. These depolarizations can generate radially directed current flow through extracellular space with the establishment of a transretinal potential.

Support for this hypothesis has come from several laboratories. Dick and Miller (10, 11), Kline et al. (21), and Karwoski and Proenza (20) have all observed light-evoked $[K^+]_o$ increases in two retinal laminae using K^+-selective micropipettes: a transient increase in the outer plexiform layer and a more prolonged increase in the distal portion of the inner plexiform layer. Current source-density studies by Newman (29, 30) demonstrate that b-wave currents originate primarily from a current source near the inner limiting membrane and from two current sinks. The locations and time courses of the two current sinks correspond closely to the time courses and locations of the two light-evoked $[K^+]_o$ increases. This correspondence supports the hypothesis that the $[K^+]_o$ increases generate b-wave current flow.

On the other hand, a number of objections have been raised to the K^+ hypothesis of b-wave generation. Perhaps the most significant concerns the difference in time course between the b-wave and the intracellular Müller cell response (see, for instance, Refs. 14, 17). According to the K^+ hypothesis, Müller cell depolarization generates b-wave current flow. Why then is the b-wave much more transient than the Müller cell response?

A second objection has recently been raised by Yanagida and Tomita (50). They pressure ejected KCl solutions from two micropipettes positioned in different retinal laminae in order to simulate the $[K^+]_o$ increases seen during the b-wave. They found that the intraretinal potential generated by these ejections was minimal at a location between the two ejection pipettes. During the b-wave response, however, the minimal intraretinal potential occurs near the outer plexiform layer, at the location of the distal $[K^+]_o$ increase. This suggests that the distal b-wave current sink may not be generated by the $[K^+]_o$ increase seen in the outer plexiform layer.

A third objection to the K^+ hypothesis concerns the magnitudes of the light-evoked $[K^+]_o$ increases that have been measured with K^+-selective micropipettes (20, 39, 49). Compared with the proximal increase, the distal $[K^+]_o$ increase measured by some laboratories does not appear to be large enough to generate the distal b-wave current sink seen in Newman's (29, 30) current source-density studies.

The retinal components, which, according to the K^+ hypothesis, interact to generate the b-wave response, represent a complex physical system. This system includes the Müller cell, which is believed to have highly differentiated membrane properties (14, 27–30, 32, 50). Other components of the K^+ hypothesis model include time-varying cellular sources and sinks of K^+, diffusion of released K^+ through extracellular space, active uptake of K^+ from extracellular space, and K^+ drift across the Müller cell membrane. The current and voltage-generating properties of a system embodying these components is complex and cannot be analyzed through qualitative procedures alone.

We have chosen to study the properties of such a retinal system by constructing a computer model that simulates the behavior of the relevant retinal structures. Using this model, we have simulated various aspects of b-wave generation and have studied in detail the objections to the K^+ hypothesis discussed above. A summary of some of this work has appeared previously (34).

MODEL

Our model simulates retinal processes that, according to the K^+ hypothesis, generate the b-wave response. The model assumes uniformity of geometry, ion concentrations, and electric potential in planes parallel to the retinal surface. Uniformity of ion concentration and potential will occur when the retina is illuminated uniformly. Under this condition the retina can be modeled by a one-dimensional system with retinal depth as the single spatial variable (36). The model represents an idealized amphibian retina.

Our goal has been to study the general properties of the K^+ hypothesis system rather than to reproduce a single set of experimental results. Accordingly, we have chosen system parameters that are typical of the amphibian retina. Nevertheless, the results of the simulations are not significantly altered by variations in many of the system parameters (see below).

The model comprises the following components. They are summarized in Fig. 1 and Table 1.

Retina. For the purpose of specifying current flow, the retina is assumed to be in an eyecup preparation, with the pigment epithelium intact. The thickness of the retina proper is 250 μm, extending from the inner limiting membrane, 0% depth, to the distal end of the outer segments, 100% depth. The pigment epithelium extends from 100 to 106% depth.

Extracellular space. The volume fraction of extracellular space is equivalent to the cross-sectional area of extracellular space per unit cross-sectional area of whole tissue (37). In our model, the volume fraction is set to 100% in the vitreous (<0% depth) and distal to the pigment epithelium (>106% depth). Within the retina (0–100% depth) the volume fraction is 7%. Although lower than some estimates of the volume fraction in the central nervous system (37), this figure was chosen because it produced a transretinal resistance in the model retina of 78 $\Omega \cdot cm^2$, similar to the value measured experimentally in the frog retina (30; D. A. Frambach, personal communication). In the pigment epithelium layer, we assume an extracellular volume fraction of 0.07%. This restricted cross-sectional area simulates the diffusion barrier presented by the pigment epithelium membranes and associated tight junctions (7). The restricted space from 100 to 106% depth models the high-resistance "R-membrane," which has been localized experimentally to the pigment epithelium membrane (3, 46).

Experimental measurements (30, 42) show that different retinal laminae can differ somewhat in their specific resistance. Thus the uniform resistance (volume fraction) of extracellular space used in the model from 0 to 100% depth is somewhat of a simplification. However, we did use nonuniform distributions of extracellular resistance in several simulations and found that within the range tested, resistance variations changed the spatial and temporal properties of the b-wave and Müller potentials very little (see DISCUSSION section).

Extraretinal shunt resistance. In our simulations the vitreous is in indirect electrical contact with the sclera via an extraretinal shunt pathway (indicated by the arrowheads in the lower trace of Fig. 1) (see, for instance, Ref. 45). This pathway simulates the shunt resistance that occurs in the intact eye and in eyecup preparations and that leads to a reduction in light-evoked transretinal voltages. Except when otherwise noted, the shunt resistance in the model (from 0% depth through the vitreous and back to 106% depth) is 1,400 $\Omega \cdot cm^2$.

Diffusion and extracellular ion concentrations. The K^+ diffusion coefficient, D_K, is assumed to equal $2 \cdot 10^{-5}$ cm^2/s in our model, the value measured in saline (15). Within the retina and pigment epithelium (0–106% depth) the effective diffusion coefficient of K^+ in extracellular space is reduced

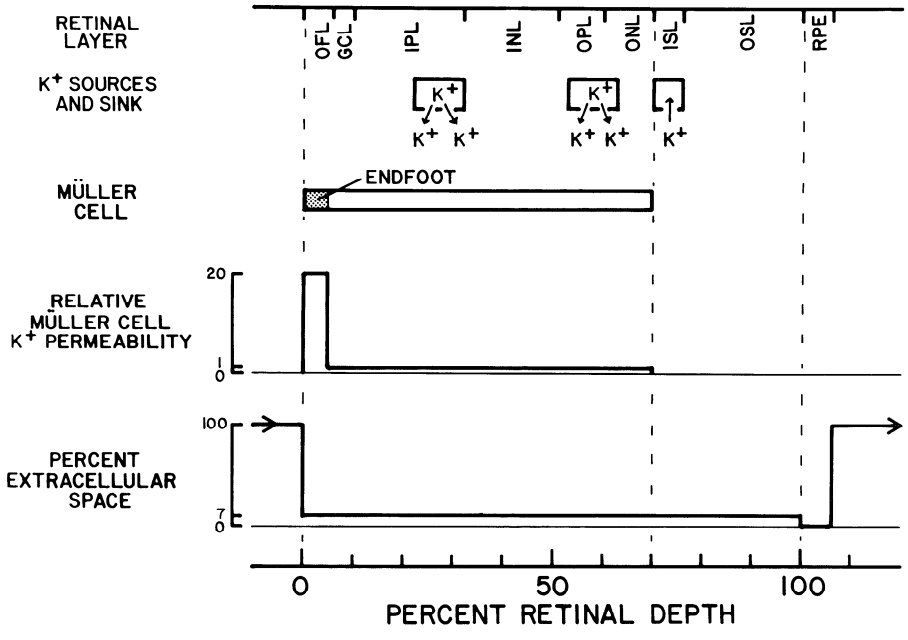

FIG. 1. Summary of retinal model. Locations and values of retinal structures and parameters are shown as a function of percent retinal depth. Retinal layers, shown above plots are, from left to right, optic fiber layer, ganglion cell layer, inner plexiform layer, inner nuclear layer, outer plexiform layer, outer nuclear layer, (rod) inner segment layer, (rod) outer segment layer, and retinal pigment epithelium layer.

TABLE 1. *Model parameters and assumptions*

Parameter	Value in Model	Range of Values Tested
Retinal depth (0–100%)	250 μm	
Extracellular volume fraction (of total retinal volume)		
In vitreous and beyond pigment epithelium	100%	
In retina (0–100% depth)	7%	100% for damaged retina
In pigment epithelium (100–106% depth)	0.07%	
$[K^+]_o$ (initial)	2.5 mM	
$[Na^+]_o$	100 mM	
$[Cl^-]_o$	102.5 mM	
Retinal resistivity (0–100% depth)	3,125 $\Omega \cdot$ cm	1,562–6,250 $\Omega \cdot$ cm (in nuclear layers)
Retinal resistance		
From 0–100% depth	78 $\Omega \cdot cm^2$	
From 0–106% depth	547 $\Omega \cdot cm^2$	
Extraretinal shunt resistance	1,400 $\Omega \cdot cm^2$	280–7,000 $\Omega \cdot cm^2$
D_K, D_{Na}, D_{Cl} (apparent)		
In vitreous and beyond pigment epithelium	$2 \cdot 10^{-5}$ $cm^2 \cdot s^{-1}$	
In retina	$6 \cdot 10^{-6}$ $cm^2 \cdot s^{-1}$	$3–12 \cdot 10^{-6}$ $cm^2 \cdot s^{-1}$
Time constant of active K^+ reuptake	10 s	
b-Wave K^+ source-sink locations		
Proximal source	22–32% depth	
Distal source	53–63% depth	
Distal sink	70–76% depth	
Uptake rate constant of K^+ sink	0.4 s^{-1}	
Müller cell		
Location, entire cell	0–70% depth	
Location, endfoot	0–5% depth	
K^+ membrane permeability ratio of endfoot versus remainder of cell (per unit depth)	20:1	1:1–60:1
Electrical length constant	166 μm	
Volume fraction (of total retinal volume)	7%	1.4–35%
$[K^+]_i$	100 mM	
$[Cl^-]_i$	100 mM	

by a factor λ^2, where λ is the tortuosity factor (35, 37). λ = 1.8 in our model, a value close to that measured experimentally for small ions (37). D_K (apparent) within the retina, designated D_K^*, thus equals D_K/λ^2 or $6 \cdot 10^{-6}$ cm^2/s. For simplicity, we assume that D_{Na} and D_{Cl} also equal $2 \cdot 10^{-5}$ cm^2/s and that λ = 1.8 for both these ions within the retina.

In our simulations, $[K^+]_o$ is initially set to 2.5 mM and $[Na^+]_o$ to 100 mM. Cl^-, the counterion for both K^+ and Na^+, is present at 102.5 mM concentration in extracellular space. $[Na^+]_o$ and $[Cl^-]_o$ are assumed to remain constant in time and space. Because K^+, Na^+, and Cl^- have equal mobilities in our simulation, diffusional potentials within extracellular space can be ignored.

Electrical conductivity of extracellular space (the interstitial conductivity) is calculated from values of extracellular ion concentrations and their diffusion coefficients using the Einstein relation: ion mobility, $\mu(cm^2 \cdot V^{-1} \cdot s^{-1})$ = ion diffusion coefficient/(kT/q). Thus

$$\text{conductivity (mho/cm)} = F([K^+]_o\mu_K + [Na^+]_o\mu_{Na} + [Cl^-]_o\mu_{Cl}) \quad (1)$$

(See end of this section for list of symbols.) Within the retina (0–100% depth) interstitial conductivity equals 0.32 mmho/cm.

To describe K^+ diffusion through the retina we take into account the variation (with depth) of the volume fraction of extracellular space (α) and membrane K^+ permeability, which affects passive K^+ diffusion and electrically driven K^+ drift across the Müller cell membrane. We also include a term to account for active ion uptake. Active uptake is assumed to occur with first-order kinetics, having a time constant of 10 s, the value derived by Karwoski and Proenza (19) in their study of K^+ distributions in the retina. Active uptake in our simulations is restricted to the region from 0 to 70% depth, i.e., within the neural retina. (A second K^+ uptake pump is located in the rod inner segment region, 70–76% depth, but is neutralized by passive K^+ efflux prior to rod hyperpolarization. See below.)

Since our transretinal electric fields are small, we need not solve the complete electrodiffusion equation. Instead we use a coupled diffusion coefficient to account for electrical interaction between K^+ and its counterion. Since K^+ and Cl^- are assumed to have equal diffusion coefficients, the coupled diffusion coefficient equals the K^+ diffusion coefficient.

The calculation of K^+ distribution with depth, incorporating diffusion through extracellular space, active uptake, and diffusion and passive drift across the Müller cell membrane, is solved in steps of 1% retinal depth. For the jth depth interval, the K^+ concentration satisfies the equation

$$\frac{d[K^+]_o}{dt} = D^*_{K,j}\frac{d^2[K^+]_o}{dz^2} - [K^+]_o\left(\frac{1}{\tau_{p,j}\alpha_j} + \frac{1}{\tau_a}\right) - \frac{G_{m,j}}{F\alpha_j}(\Delta V_j) \quad (2)$$

The differential terms in the formula are the familiar bulk diffusion equation (Fick's law). The remaining three terms account for transmembrane K^+ fluxes (diffusion, active uptake, and passive drift). In the passive diffusion term, $1/\tau_p$ is proportional to membrane permeability. α_j is the local volume fraction of extracellular space. The active term, τ_a is the time constant of active uptake (10 s). In the drift term, G_m is the total membrane conductance per unit volume of tissue and ΔV is the K^+ driving potential, the difference between the K^+ equilibrium potential and the membrane potential.

Because cell membranes are thin relative to the dimensions of the system, steady-state transmembrane concentration profiles are established rapidly ($<10^{-3}$ s) relative to other times of interest. Therefore we treat transmembrane concentration profiles and ion fluxes as if they are always in the steady state (quasi-steady-state assumption; see Ref. 25).

K^+ sources and sinks. Light-evoked changes in $[K^+]_o$ during the b-wave are simulated in the model by two K^+ sources, located between 22 and 32% depth and between 53 and 63% depth, and by a K^+ sink located between 70 and 76% depth. The two sources and the sink model the experimentally measured $[K^+]_o$ increases in the inner and outer plexiform layers and the $[K^+]_o$ decrease in the rod inner segment layer. The locations of the sources and the sink used in the simulations were chosen to match the locations of the experimentally measured $[K^+]_o$ increases and the $[K^+]_o$ decrease (10, 21, 41) and the measured distribution of the two b-wave current sinks (30). The source-density amplitude of each source and sink is assumed to be uniform across its entire width, i.e., it is spatially rectilinear.

In our simulations, K^+ source and sink values are specified for each 50-ms interval (500-ms intervals when calculating slow PIII potentials). For each time interval, the appropriate amount of K^+ is either added to or subtracted from local extracellular space. As source or sink activity progresses, $[K^+]_o$ changes accumulate. Thus, extracellular space acts as an "integrator" for source and sink activity. The integration process is "leaky" because $[K^+]_o$ changes are dissipated by diffusion, drift, and reuptake processes.

K^+ sources. K^+ efflux from the two K^+ sources is directly proportional to the value of the source density. Source magnitudes may be thought of as paralleling the amplitudes of the light-evoked responses of depolarizing retinal neurons (17).

K^+ sink. K^+ sink dynamics in our simulations are based on the model of Matsuura et al. (24) and Oakley et al. (40). Net K^+ influx is the sum of an inward K^+ flow generated by an active K^+ pump and an outward, passive K^+ flow. The active K^+ influx is assumed to be proportional to $[K^+]_o$ (over the range 2.0–3.0 mM), as is suggested from pump-activity experiments in axons (2). The passive K^+ efflux is proportional to the K^+ driving potential, the difference between the rod membrane potential (V_m) and the rod K^+ equilibrium potential (V_K). Net K^+ influx is described by the equation

$$K^+_{influx} = c[K^+]_o - \frac{G}{F}(V_m - V_K) \quad (3)$$

The first term on the right-hand side of the equation represents active K^+ influx. The parameter c is an uptake rate constant having the value 0.4 s^{-1}. The second term represents passive K^+ efflux. G represents total membrane conductance per unit volume of tissue (in units of $S \cdot cm^{-3}$). In our simulations, $V_m = -30$ mV prior to light stimulation and $V_K = -55$ mV.

Prior to a light stimulus the inward and outward K^+ fluxes are in balance and $K_{influx} = 0$. Light-evoked rod hyperpolarization drives V_m closer to V_K, reducing the passive K^+ efflux. A net current influx results. A step change in V_m produces a near exponential change in $[K^+]_o$ having a "time constant" of 3.0 s, somewhat smaller than the value

measured experimentally in the isolated retina by Oakley et al. (40).

Müller cell. The Müller cell extends from 0 to 70% retinal depth in the model, from the inner to the outer limiting membranes. It has a $[K^+]_i$ of 100 mM. With a $[K^+]_o$ of 2.5 mM, the cell has an initial membrane potential of −93 mV, similar to the value measured experimentally (31). $[K^+]_i$ is assumed to remain constant during changes in membrane potential generated by variations in $[K^+]_o$. The cell has a volume fraction (cross-sectional area of intracellular space per unit cross-sectional area of total tissue) of 7%, close to the value measured experimentally in a number of species (43). D_K^* within the Müller cell equals $2 \cdot 10^{-5}$ cm^2/s ($\lambda = 1.0$). Variations in the value of the Müller cell volume fraction (which controls cytoplasmic resistance) has relatively small effects on b-wave and Müller potentials (see DISCUSSION section).

In accord with experimental observations (31), the Müller cell membrane is assumed to be exclusively permeable to K^+. Furthermore, membrane permeability (per unit depth) is assumed to be 20 times greater in the region from 0 to 5% depth than it is in the region from 5 to 70% depth. This permeability distribution is in accord with a number of recent physiological studies of Müller cell membrane properties (14, 27–32, 48, 50), all of which indicate that a large fraction of total Müller cell K^+ permeability is located in the endfoot region of the cell. This skewed permeability distribution seen experimentally could be due to a specialization of endfoot membrane conductance properties, to a large increase in membrane surface area in the endfoot region (43), or to both factors. Our choice of distributing the high-permeability region over the proximal 5% of retinal depth is not critical. Varying the width of this region over a range of 1–10% depth changes the results of our simulations little (see Ref. 30). The magnitude of endfoot permeability used in the model (20×) was chosen to produce the best fit between simulated and experimentally determined (30) b-wave current source-density plots. The electrical length constant of the model Müller cell to depolarization at 65% depth is 166 μm.

Potentials and currents. Under the quasi-steady-state assumption for transmembrane ion concentrations, we can calculate the Müller cell membrane potential at any time from the Nernst equation and the electrical properties of the retina. For example, at the jth depth step the local K^+ diffusion potential is

$$V_j = \frac{RT}{F} \ln \frac{[K^+]_{o,j}}{[K^+]_i} \qquad (4)$$

The distribution of potential in the extracellular space, like the diffusion calculation, is solved in steps of 1% retinal depth. For the jth step, the distribution of potential is derived from the circuit diagram, Fig. 2, where $R_{e,j}$ and $R_{i,j}$ are the extracellular and intracellular resistances in interval j, $R_{m,j}$ is the Müller cell membrane resistance in interval j, V_j is the Müller cell K^+ diffusion potential in interval j, i_j is the mesh current flowing within interval j, and i_s is the mesh current flowing through the extraretinal shunt resistance. R_e, R_i, and R_m are calculated from the local values of *1*) the concentrations and mobilities of K^+, Na^+, and Cl^- (as described in *equation 1*); *2*) the volume fraction of extracellular space; *3*) the volume fraction of the Müller cell; and *4*) the Müller cell membrane permeability. V is calculated from *equation 4*. Once these values are tabulated, the mesh currents, i_j, and the shunt current, i_s, are calculated using equations given in the APPENDIX. The local Müller cell membrane potential is the sum of the Nernst potential (V) and the voltage resulting from current flow through the membrane resistance. Based on this network of resistances and voltage sources, the model computes current flows and associated potential drops across the entire depth of the retina. Details of these calculations are given in the APPENDIX.

In summary, for a specified temporal pattern of K^+ source-density for the two K^+ sources and the K^+ sink, the spatiotemporal distribution of $[K^+]_o$ is calculated. Based on this K^+ distribution, the model computes the Müller cell potential, extracellular potentials, and the current source-density in both space and time. Calculations were performed on a Digital Equipment Corp. PDP 11/40 computer and results displayed graphically on a Hewlett Packard 2648A graphics terminal.

Light-evoked $[K^+]_o$ and retinal damage

In addition to the calculations described above, we have simulated light-evoked $[K^+]_o$ changes that would be measured in a retina damaged by an ion-selective micropipette. Because retinal damage produced by a pipette will be localized to the pipette tip, the problem cannot be modeled in a one-dimensional system. Instead, $[K^+]_o$ levels are computed in a model that simulates damage in three dimensions. The region of damaged retinal tissue

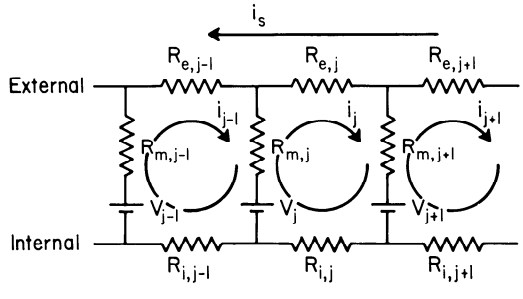

FIG. 2. Circuit diagram of retinal model.

is restricted to a cylindrical volume of diameter and length, d. Within this region the volume fraction of extracellular space is increased to 100%, the tortuosity factor is reduced to 1.0 (thus increasing D_K (apparent) to $2 \cdot 10^{-5}$ cm^2/s), and any K^+ sources or sinks are eliminated.

$[K^+]_o$ levels within the damaged region are computed as a function of time using a coupled transmission line model. Within the damaged region, K^+ diffusion along the depth axis of the retina is computed as described above by *equation 2*. An additional term is included to account for K^+ diffusing in tangential planes from the undamaged retina into the damaged region. The magnitude of this term is estimated by assuming that $[K^+]_o$ outside the damaged region is uniform in tangential planes and equal to $[K^+]_o$ in an undamaged retina. The magnitude of K^+ diffusion into the damaged region is calculated for each depth increment from an equation describing diffusion into a disk of diameter d lying in an infinite plane (see Ref. 9, p. 30). For this calculation, the initial value of $[K^+]_o$ within the disk is set to the $[K^+]_o$ value at the middle of the damaged region at the previous time step. The initial value of $[K^+]_o$ outside the disk equals $[K^+]_o$ in the undamaged retina at the previous time step. This estimate of the coupling between damaged and undamaged tissue will overestimate somewhat the amount of K^+ diffusing into the damaged region.

List of symbols

c	uptake rate constant of K^+ sink, s^{-1}
d	diameter of damaged retinal region, μm
D	ion diffusion coefficient, $cm^2 \cdot s^{-1}$
D*	D (apparent), D/λ^2, $cm^2 \cdot s^{-1}$
F	Faraday constant, $C \cdot mol^{-1}$
G	conductance/cm of rod membrane, $S \cdot cm^{-3}$
G_m	conductance/cm of Müller cell membrane, $S \cdot cm^{-3}$
i_j	mesh current in interval j, A
i_s	mesh current in extraretinal shunt pathway, A
k	Boltzmann constant, $J \cdot K^{-1}$
$[K^+]_o$, $[Na^+]_o$, $[Cl^-]_o$	extracellular ion concentration, M
$[K^+]_i$, $[Cl^-]_i$	Müller cell intracellular ion concentration, M
q	elementary charge, C
R	gas constant, $J \cdot mol^{-1} \cdot K^{-1}$
$R_{e,j}$	external resistance in interval j, Ω
$R_{i,j}$	internal resistance in interval j, Ω
$R_{m,j}$	Müller cell membrane resistance in interval j, Ω
R_s	extraretinal shunt resistance, Ω
t	time, s
T	temperature, K
V	Müller cell K^+ potential, V
V_K	rod K^+ potential, V
V_m	rod membrane potential, V
z	retinal depth, cm
α	volume fraction of extracellular space, dimensionless
μ	mobility, $cm^2 \cdot V^{-1} \cdot s^{-1}$
τ_a	time constant of active K^+ uptake, s
τ_p	time constant of passive K^+ diffusion through Müller cell membrane (inversely proportional to membrane permeability), s
λ	tortuosity factor, dimensionless

RESULTS

The b-wave is simulated in our model system using the K^+ source and sink values illustrated in Fig. 3. Amplitudes of the two K^+ sources are shown as a function of time in Fig. 3*A*. The K^+ sink curve in Fig. 3*B* indicates the imposed time course of rod hyperpolarization which, in turn, drives the current sink

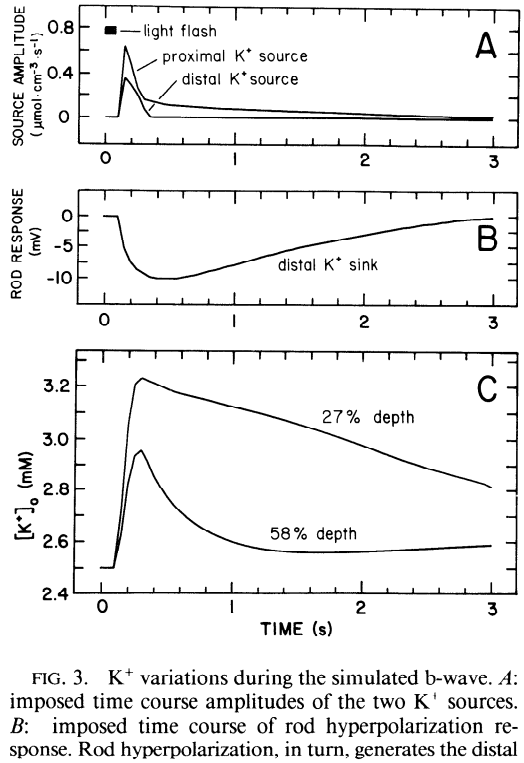

FIG. 3. K^+ variations during the simulated b-wave. *A*: imposed time course amplitudes of the two K^+ sources. *B*: imposed time course of rod hyperpolarization response. Rod hyperpolarization, in turn, generates the distal K^+ sink as specified by *equation 3* (MODEL section). *C*: $[K^+]_o$ variations resulting from the K^+ source-sink activity specified in *A* and *B*. The two traces represent $[K^+]_o$ at 27 and 58% retinal depths, the midpoints of the two K^+ sources. The rapid return to base line at 58% depth is caused by "diffusion" of the distal $[K^+]_o$ decrease into the outer plexiform layer.

(see above). The variations in $[K^+]_o$ in time resulting from the two K^+ sources and the K^+ sink are illustrated in Fig. 3*C*. They represent $[K^+]_o$ values at 27 and 58% depths, the midpoints of the two K^+ sources. The distal $[K^+]_o$ increase is both smaller in magnitude and more transient in time course than the proximal increase. This reproduces the properties of the light-evoked K^+ changes that have been measured experimentally with K^+-selective micropipettes. (Although some investigators, notably Kline et al. (21), have measured a distal $[K^+]_o$ increase nearly as large as the proximal one, other workers (10, 18) have seen only small distal increases. We justify our choice of a relatively large distal increase for modeling b-wave generation in the DISCUSSION section.)

The temporal and spatial variations in $[K^+]_o$ illustrated in Fig. 3*C* produce changes in the Müller cell membrane potential and generate radially directed currents within the retina. The intracellular Müller cell response and the transretinal potential that are generated by our model system are illustrated in Fig. 4. The Müller cell potential represents the intracellular voltage measured at the cell body (42% depth) and referenced to the extracellular potential at 0% depth. The b-wave potential is the extracellular voltage at 0% depth referenced to the extracellular voltage at 110% depth (a point just beyond the pigment epithelium). This potential is equivalent to the ERG voltage measured between the vitreous and the sclera in an eyecup preparation.

The rising phase of the Müller potential

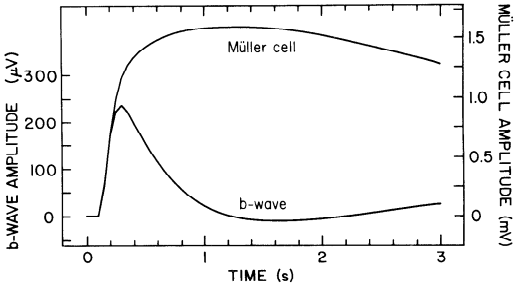

FIG. 4. Time course of retinal responses. Müller cell plot represents the intracellular potential at 42% depth referenced to the extracellular potential at 0%. The Müller cell resting potential is −93 mV. The b-wave plot represents the extracellular potential difference between 0 and 110% depth. The b-wave potential decays much more rapidly than does the Müller cell response.

and the ERG potential have similar time courses in our simulation. However, the remainder of the two potentials differ dramatically. The Müller cell response remains large for several seconds, decaying only slowly. The b-wave response, on the other hand, decays to near base line within the first second of the response.

The magnitude and duration of the distal K^+ sink has a strong influence on the time course of the transretinal b-wave response in our model system. Decreasing K^+ sink magnitude (reducing imposed rod hyperpolarization) produces a b-wave response that decays more slowly. A large, prolonged distal K^+ sink, on the other hand, leads to a b-wave with a shorter decay phase than that shown in Fig. 4.

The distribution of $[K^+]_o$, current source-density, and intraretinal potential, all plotted as a function of retinal depth, are illustrated in Fig. 5. These distributions were calculated at a time corresponding to the b-wave peak (300 ms), using the K^+ source and sink values shown in Fig. 3. The spatial distribution of $[K^+]_o$ (Fig. 5*A*) shows two major peaks of increased $[K^+]_o$. These are generated by the two K^+ sources. These two high $[K^+]_o$ regions depolarize the Müller cell membrane locally, generating local current influx. This is illustrated in the current source-density plot (Fig. 4*B*), which shows two prominent current sinks at the same depths as the $[K^+]_o$ increases. A large fraction of the current entering the Müller cell from these two sinks exits from the current source at the endfoot region of the cell (0–5% depth). Current flows preferentially across this region of cell membrane because its permeability to K^+ is 20 times greater per unit depth than other portions of the cell. The current efflux in the endfoot region is carried by K^+ ions and thus represents a secondary K^+ source. As shown in Fig. 5*A*, this source raises $[K^+]_o$ in the region from 0 to 10% depth.

The current entering the Müller cell at the two current sinks and exiting from the current source establishes a current flow directed distally in extracellular space. This current, flowing through the extracellular resistance, establishes an intraretinal potential (Fig. 5*C*). The potential falls steadily from a maximal value at 0% depth and reaches a minimum in the distal retina at 60% depth, near the border of the outer plexiform and outer nu-

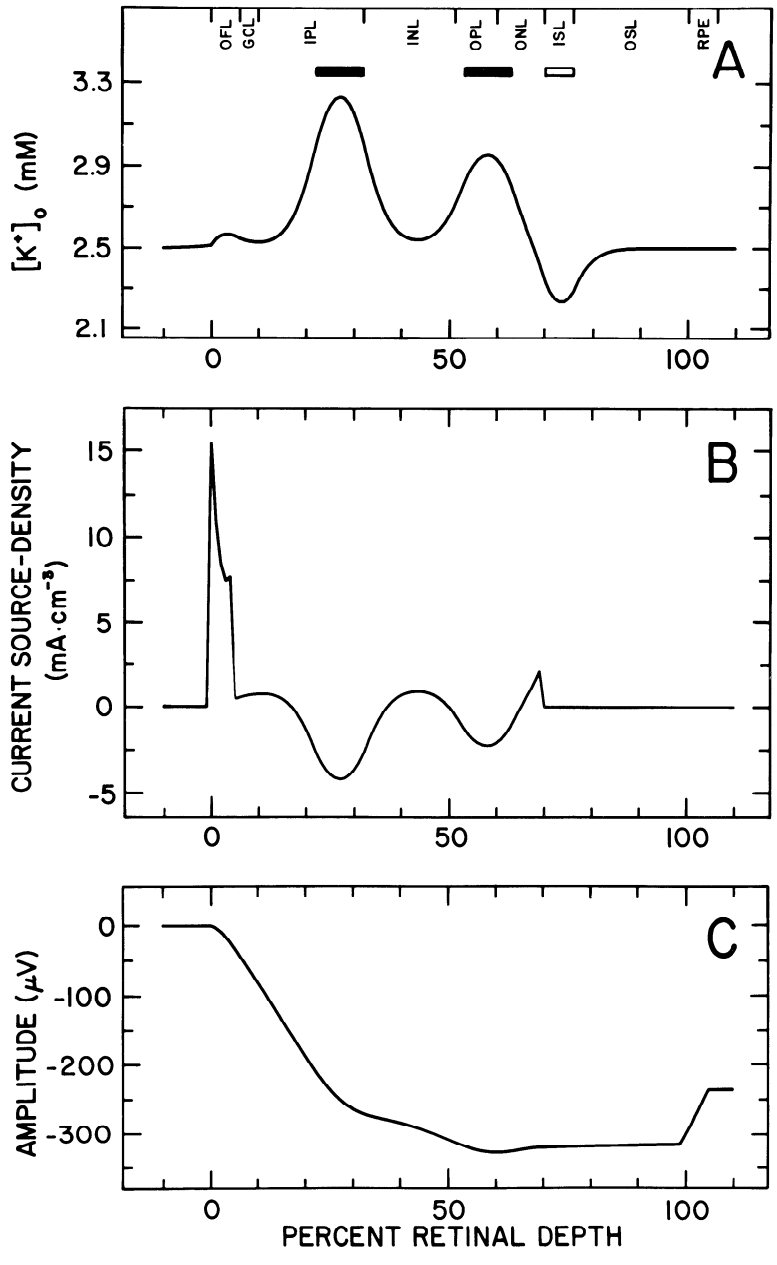

FIG. 5. Intraretinal b-wave depth profiles computed at 300 ms, the peak of the response. *A*: $[K^+]_o$ versus retinal depth. Locations of the retinal layers and the K^+ sources (filled bars) and sink (open bar) are shown above the plot. *B*: current source-density distribution. b-Wave current arises primarily from current sinks in the inner and outer plexiform layers and from a current source in the proximal 5% of the retina. *C*: b-wave amplitude. The b-wave potential reaches a minimal value near the border of the outer plexiform and outer nuclear layers. The rise in the potential in the extreme distal retina (100–106% depth) represents the voltage drop produced by b-wave shunt current flowing across the high-resistance pigment epithelium membranes.

clear layers. The rise in potential in the region from 100 to 106% depth occurs as the current flowing through the extraretinal shunt pathway flows through the high-resistance membranes of the pigment epithelium.

The spatial distributions of $[K^+]_o$, current

source-density, and potential illustrated in Fig. 5 strongly resemble experimentally measured values. K^+-selective micropipette measurements reveal two regions of $[K^+]_o$ increase, in the distal inner plexiform layer and in the outer plexiform layer (10, 11, 20, 21), and a distal decrease in $[K^+]_o$ in the inner segment layer (41). Experimentally determined current source-density distributions show two current sinks, also in the distal inner plexiform and outer plexiform layers, and a large current source at the inner surface of the retina (29, 30). The three secondary sources of b-wave current seen in Fig. 5*B* between and flanking the two current sinks have also been observed experimentally (12, 30). Numerous measurements of the intraretinal b-wave potential show that it is maximal at the retinal surface and reaches a minimum near the outer plexiform layer (4, 12, 29, 47).

Extraretinal shunt pathway

Our simulations demonstrate that the spatial distribution of the intraretinal b-wave potential is sensitive to the magnitude of the extraretinal shunt resistance (see also Refs. 16, 45). This phenomenon is illustrated in Fig. 6. When the shunt resistance is increased from the nominal level (trace b) to a fivefold higher value (trace c), there is a marked reduction in the current flow and, hence, a reduction in the voltage drop across the pigment epithelium membranes. When the shunt resistance is decreased to one-fifth the normal value (trace a), the magnitude of the current flow across the pigment epithelium increases. This produces a large voltage drop across the pigment epithelium membranes.

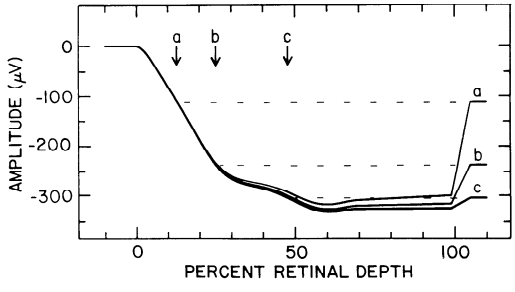

FIG. 6. Intraretinal b-wave depth profiles (computed at 300 ms) for three values of extraretinal shunt resistance. The b-wave potential computed using the normal shunt resistance is shown by trace b. When shunt resistance is reduced to 20% the normal value (a), the voltage drop across the high-resistance pigment epithelium (100–106% depth) is increased. When shunt resistance is increased to a high value (c, 500% the normal value), the voltage drop across the distal retina is very small. Arrows indicate locations of the reversal points, where the b-wave potential shifts from a positive to a negative response when referenced to the distal extreme of the retina. The location of the reversal point shifts proximally as the extraretinal shunt resistance is reduced.

The most dramatic effect of decreasing the extraretinal shunt resistance in our simulations is to decrease the amplitude of the transretinal b-wave voltage (the potential difference between 0 and 110% depth). Decreasing the shunt resistance also decreases the peak negative intraretinal potential slightly.

Another consequence of the change in shunt resistance is to shift the location of the "reversal point" of the intraretinal potential (indicated by arrows in Fig. 6). This is the location within the retina where the b-wave shifts from a positive to negative potential, when the response is referenced to the sclera (or to the distal extreme of the retina). As shown in Fig. 6, the reversal point is located more distally when the intraretinal shunt resistance is high and more proximally when the shunt resistance is low. (There is, of course, no reversal point when the intraretinal b-wave is referenced to the vitreous. It is always negative.) The simulation shown in Fig. 6 demonstrates that the location of the reversal point of the sclerally referenced b-wave has no inherent meaning in itself. It simply reflects the magnitude of the extraretinal shunt resistance.

K^+ ejection experiments

Tomita and his colleagues (14, 48, 50) have investigated the effects of intraretinal ejections of K^+ solutions on intraretinal and transretinal potentials. They have analyzed their results in terms of the K^+ hypothesis, assuming that the potentials resulting from the ejections arise from K^+-generated current flow through Müller cells.

We have simulated their experiments in our model system, using short pulses of a K^+ source to simulate the pressure-ejected K^+ used in the experimental preparations. All other model parameters are identical to those used in our b-wave simulations. Our simulations do not reproduce the experiments precisely. Our model assumes that K^+ diffusion and current flow occurs only in a radial direction, while in the original experiments,

ejected K^+ is free to diffuse (and current to flow) tangentially as well as radially within the retina. Our one-dimensional approximation is sufficient to investigate the phenomena of intraretinal K^+ ejections qualitatively, however, and, in fact, reproduces the experimental data quite well.

SINGLE K^+ EJECTIONS. Fujimoto and Tomita (14) measured intraretinal voltage responses generated by K^+ ejections at different retinal depths. We simulated these experiments by locating a single K^+ source at specified locations within the retina. Our K^+ stimulus was a 50-ms pulse of K^+ ejected into extracellular space. The intraretinal potentials resulting from these ejections were measured after a delay of 300 ms.

Fujimoto and Tomita (14) found that intraretinal K^+ ejections resulted in the generation of a vitreal-positive transretinal potential for all but the most proximal locations of the ejection pipette. Only when the K^+ pipette was positioned within 10–20 μm of the inner limiting membrane was a vitreal-negative response generated. This finding is reproduced qualitatively in our model. Simulated K^+ ejections from 1 to 20% depth produce vitreal-negative transretinal potentials (the potential at 0% depth is more negative than at 110% depth), while ejections at all depths distal to 21% produce vitreal-positive responses. The "neutral point," where K^+ ejection elicits neither a positive nor a negative transretinal potential, is located at 21% depth in our model.

Fujimoto and Tomita (14) point out that the asymmetric location of the neutral point indicates that a large fraction of the Müller cell K^+ permeability is localized near the inner limiting membrane. In our simulation, the location of the neutral point depends strongly on the permeability of the Müller cell endfoot region. When the permeability of the Müller cell from 0 to 5% depth is decreased 20-fold, to the value of the remainder of the cell, the neutral point shifts from 21% depth to 35% depth, the precise midpoint of the cell. On the other hand, the location of the neutral point shifts from 21 to 17% depth when the permeability of the Müller cell membrane from 0 to 5% depth is raised threefold, from 20 to 60.

DOUBLE K^+ EJECTIONS. Tomita and Yanagida (48) and Yanagida and Tomita (50) have simulated the two K^+ sources seen during the b-wave response by pressure ejecting K^+ from a pair of pipettes positioned in different retinal layers. We have, in turn, simulated their experimental results by locating two K^+ sources at 25 and 48% depths in our model system. These correspond approximately to the locations of the two pressure-ejection pipettes used by Tomita and Yanagida.

The intraretinal potentials generated by our model for the two K^+ sources activated separately and for both activated together are illustrated in Fig. 7*A*. For the single K^+ sources, the potential profile reaches a minimum near the site of the K^+ source. When both K^+ sources are activated simultaneously, the minimum of the potential is located between the two K^+ sources. Tomita and Yanagida

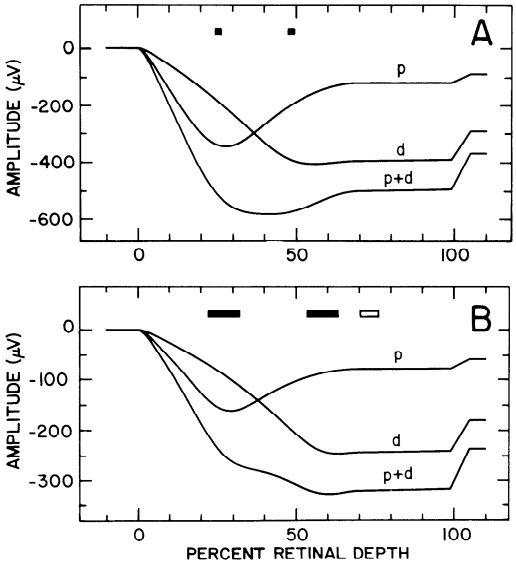

FIG. 7. Intraretinal voltage profiles generated by paired K^+ sources. *A*: response profiles for simulated K^+ ejections at 25% depth (p), 48% depth (d), and for combined proximal and distal ejections (p + d). Response profiles are computed after a 300-ms delay from the time of ejection. The potential representing the combined ejection (p + d) reaches a minimal value at a location between the two ejection sites (filled bars). *B*: voltage profiles for b-wave K^+ sources and sink. K^+ source-sink time courses are the same as those shown in Fig. 3. Illustrated here are response profiles generated by the proximal K^+ source alone (p), by the distal K^+ source and the distal K^+ sink (d), and for all three together (p + d). Response profiles are computed at 300 ms. The p + d potential reaches a minimal value near the location of the distal K^+ source. Locations of the K^+ sources (filled bars) and the K^+ sink (open bar) are shown above the graph.

(48) obtained similar results in their experimental system.

A similar simulation is illustrated in Fig. 7*B*. However, instead of using two-point sources of K^+, we have specified locations and time courses of two K^+ sources and a K^+ sink that are appropriate for the b-wave (those shown in Fig. 3).

The intraretinal potentials generated by the proximal K^+ source and by the distal K^+ source and sink activated separately have minimal values near the locations of the two K^+ sources. When both K^+ sources are activated together, however, the minimum value of the intraretinal potential is located in the distal retina at the location of the distal K^+ source.

There is a qualitative difference between the profiles of intraretinal potentials in the two simulations. When Tomita and Yanagida's (48) experiment is modeled, the intraretinal potential peaks between the two K^+ sources. When the b-wave is modeled, the potential peaks near the distal K^+ source. The simulations accurately reproduce both sets of experimental results.

Slow PIII response

The slow PIII response, as well as the b-wave, is believed to be generated by an interaction between varying $[K^+]_o$ levels and Müller cells (12). Specifically, the vitreal-negative slow PIII is thought to be generated by Müller cell hyperpolarization in response to the $[K^+]_o$ decrease arising from the rod inner segment layer. We have simulated the generation of the slow PIII response in order to test the general applicability of our model retinal system.

We generated slow PIII responses using the distal K^+ sink alone, specifying the time course of rod hyperpolarization. All system parameters are identical to those used in the b-wave simulations.

One example of imposed rod hyperpolarization is shown in Fig. 8*A*. It represents the response of a dark-adapted rod to a brief light flash. The simulated rod response, with its plateau and slow-decay phases, was chosen to match an experimentally measured rod response (40).

The decrease in $[K^+]_o$ generated by the rod hyperpolarization is illustrated in Fig. 8*B*. It represents $[K^+]_o$ levels at 73% depth, the midpoint of the rod inner segment layer. The $[K^+]_o$ decrease reaches a minimum after the rod response begins to decay. The same temporal relation between rod potential and $[K^+]_o$ has been noted experimentally (40).

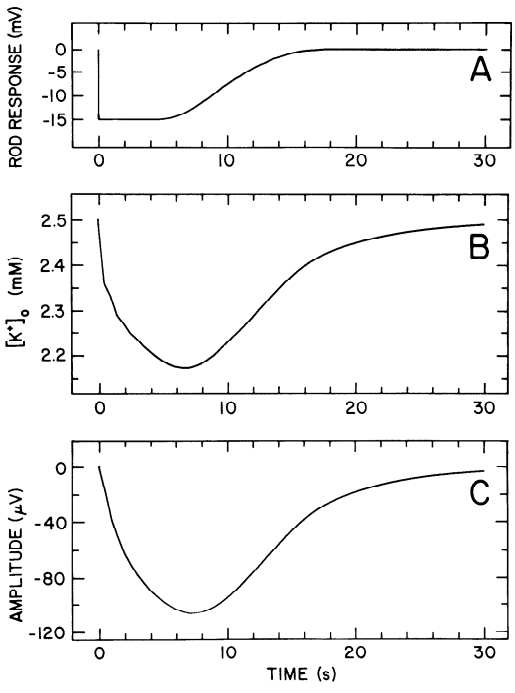

FIG. 8. Generation of the slow PIII potential. *A*: imposed time course of rod hyperpolarization. The response generates a distal K^+ sink as specified by *equation 3* (MODEL section). The proximal and distal K^+ sources are not used in this simulation. *B*: resulting $[K^+]_o$ decrease measured at 73% depth, the midpoint of the distal K^+ sink. The $[K^+]_o$ response does not peak until after the rod response begins to decay. *C*: extracellular transretinal potential generated by the $[K^+]_o$ decrease. This vitreal-negative potential has a time course typical of the slow PIII response. The delay between the $[K^+]_o$ decrease and the transretinal potential is due to diffusion of the $[K^+]_o$ decrease into the region of the Müller cell.

The transretinal potential generated by the $[K^+]_o$ decrease is shown in Fig. 8*C*. It is a vitreal-negative response having a time course similar to experimentally recorded slow PIII potentials (12, 33). The simulated slow PIII response peaks at a somewhat later time than does the $[K^+]_o$ decrease measured at 73% depth. The difference in peak latencies represents the delay introduced by K^+ diffusion from the rod inner segment layer to the Müller cell. A similar delay in peak latencies has been noted between the $[K^+]_o$ decrease and the c-

wave (39). In the latter case, the delay is caused by K^+ diffusion from the inner segment layer to the pigment epithelium apical membrane (41).

DISCUSSION

Several previous attempts have been made to account for b-wave generation based on the principles of the K^+ hypothesis. Karwoski and Proenza (17, 18) and Oakley (39) concluded from qualitative reasoning that the time course as well as the intraretinal distribution of the b-wave potential could not arise solely from a $[K^+]_o$ increase in the proximal retina. They did not include a distal $[K^+]_o$ increase in their treatments. Kline et al. (21) treated the influence of both a proximal and a distal $[K^+]_o$ increase on intraretinal voltage but did not consider the effects of the large Müller cell K^+ permeability in the endfoot region. Thus, they postulated that the proximal K^+ increase generates a vitreal-negative transretinal response. This is most probably incorrect, as demonstrated by Newman's (29, 30) current source-density analyses and, most notably, by Fujimoto and Tomita's (14) K^+ ejection experiments. Vogel (49) analyzed b-wave generation using measurements of both $[K^+]_o$ levels and current source-density distributions. However, his treatment did not include the distal $[K^+]_o$ increase or the large b-wave current source at the inner limiting membrane.

None of these previous analyses modeled b-wave generation in a quantitative fashion. The diffusion of K^+ through extracellular space was not considered; neither were the effects of a regional variation in Müller cell K^+ permeability. These factors influence the time course of the b-wave and Müller cell responses significantly.

We have attempted, in our model, to incorporate all factors that we believe have a significant effect on b-wave generation. The responses generated by this model are in close agreement with experimental findings. Given reasonable values of K^+ source-density for the K^+ sources and sink, b-wave and Müller cell responses with the proper time courses are generated. The resulting distribution of current source-density and intraretinal b-wave potentials closely resemble experimentally measured values. In addition, the model accurately simulates intraretinal voltages generated by experimental ejection of K^+ by single and paired intraretinal micropipettes, and simulates the generation of the slow PIII potential.

Variations in system parameters

It might be argued that the responses generated by the model have the proper temporal and spatial characteristics only because of judicious choice of system parameters. In fact, the properties of the model system are changed little when the values of system parameters are altered within ranges consistent with experimental observation. We stress that all of the simulations reported here, including b-wave, Müller cell, K^+ ejection, and slow PIII potentials, are generated using identical system parameters. Only the values of the K^+ sources and sink are changed to produce the different responses.

The influence of several system parameters on b-wave generation were examined in detail.

EXTRACELLULAR RESISTANCE. The resistance of extracellular space has been assumed to be constant from 0 to 100% depth. However, the spatial and temporal characteristics of the simulated b-wave and Müller cell responses are altered little when the resistance of the inner and outer nuclear layers is either doubled or halved from its nominal value. (These resistance changes were produced in these tests without altering the volume fraction of extracellular space.) These imposed variations in resistance more than account for the laminar differences in retinal resistance noted by Proenza and Freeman (42).

HIGH-RESISTANCE R-MEMBRANE. The R-membrane is located in the pigment epithelium layer (100–106% depth) in our simulations. However, this high-resistance region is found to extend into the outer-segment layer in some experimental preparations (12, 30). When this more extended distribution of high resistance (the high-resistance region extending from 76 to 100% depth) is modeled, only slight temporal changes in b-wave and Müller cell potentials result. A more significant change occurs in the distribution of b-wave potential with depth. The rise in the potential in the extreme distal retina, which occurs from 100 to 106% depth in the normal model retina (Fig. 5*C*), occurs more gradually in the region from 76 to 100% depth when the location of the R-membrane is shifted.

MÜLLER CELL CYTOPLASMIC RESISTANCE. b-Wave potentials are changed only slightly when the cross-sectional area of the Müller cell is increased or decreased by a factor of 5 from its nominal value. At the lowest resistance values the Müller cell potential is nearly isopotential during the b-wave response. The internal potential becomes progressively less uniform in space as internal resistance is raised.

K^+ DIFFUSION COEFFICIENT. b-Wave and Müller cell responses are changed little when D_K (apparent) within extracellular space of the retina is raised or lowered twofold from the nominal value of $6 \cdot 10^{-6}$ cm^2/s. The most notable effect is on the falling phase of the responses, which decays at a faster rate when the diffusion coefficient is increased.

MÜLLER CELL K^+ PERMEABILITY. In contrast to the above parameters, the distribution of membrane K^+ permeability along the Müller cell is critical. When the permeability of the Müller cell endfoot (0–5% depth) is lowered 20-fold to the same value as the remainder of the cell, the b-wave is altered significantly. The transretinal b-wave potential is reduced to 20% of its normal amplitude. In addition, the spatial distributions of intraretinal b-wave potential and current source-density are dramatically altered. In particular, the proximal current source in current source-density plots (Fig. 5*B*) is marked reduced. The results demonstrate that the Müller cell endfoot must have high K^+ permeability for our simulations to recreate the current source-density distributions measured experimentally. Our simulations thus lend support to the experimental findings (27–29, 31, 32) that the Müller cell endfoot region has high K^+ permeability.

b-Wave and Müller cell response waveforms

According to the K^+ hypothesis, increased levels of $[K^+]_o$ depolarize Müller cells. These depolarizations, in turn, drive the currents that generate the b-wave. Yet the Müller cell response is far more prolonged than the b-wave. This difference between the two responses has led some investigators to question the K^+ hypothesis. However, our simulations of b-wave generation demonstrate that a prolonged Müller cell response and a transient b-wave can both arise from the processes outlined in the K^+ hypothesis. The difference in the time course between the two responses arises primarily from the differences in duration and amplitude of the proximal and distal $[K^+]_o$ increases.

B-WAVE. The b-wave response decays rapidly because it is generated primarily by the short-lived distal $[K^+]_o$ increase. The more prolonged proximal $[K^+]_o$ increase contributes little to the total transretinal potential. This occurs, even though the distal $[K^+]_o$ increase is significantly smaller than the proximal one, because the current generated by the distal increase (most of it flowing from the current source near the inner limiting membrane) falls across a large extracellular resistance within the retina.

This phenomenon is illustrated in Fig. 9*A*, which shows the time course of the transretinal b-wave potential generated by the proximal K^+ source alone (p), by the distal K^+ source and K^+ sink (d), and by all three together (p + d). The combined distal K^+ source and sink

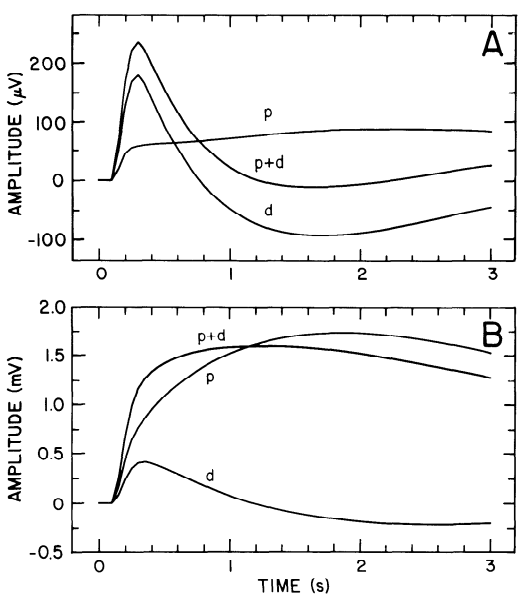

FIG. 9. Proximal and distal K^+ source responses. *A*: time course of transretinal potentials generated by the proximal K^+ source alone (p), by the combined distal K^+ source and K^+ sink (d), and by all three together (p + d). *B*: time course of the Müller cell potential generated by the proximal K^+ source alone (p), by both the distal K^+ source and K^+ sink (d), and by all three together (p + d). The b-wave response is dominated by the transient distal K^+ source and sink combination, while the Müller cell response primarily reflects the sustained proximal K^+ source.

generate a large transretinal potential that accounts for 76% of the total b-wave amplitude. The proximal source, on the other hand, produces a small sustained transretinal potential that generates only 24% of the b-wave amplitude at the peak of the response.

MÜLLER CELL RESPONSE. The Müller cell potential, in contrast to the b-wave, more closely reflects the total change in $[K^+]_o$ within the retina. It is thus dominated by the large and prolonged proximal $[K^+]_o$ increase. This is illustrated in Fig. 9*B*, which shows the Müller cell potential generated by the proximal K^+ source alone (p), by the combined distal K^+ source and K^+ sink (d), and by all three together (p + d). The sustained proximal $[K^+]_o$ increase clearly dominates the total Müller cell response. The small, transient contribution of the distal $[K^+]_o$ increase only adds significantly during the rising phase of the response.

The proximity of the high-permeability endfoot region to the proximal K^+ source further increases the proximal $[K^+]_o$ contribution to Müller cell depolarization. As K^+ released from the proximal source diffuses into the endfoot region, the depolarization generated by the $[K^+]_o$ increase is magnified.

Intraretinal K^+ ejections

Yanagida and Tomita (50), in a test of the K^+ hypothesis, pressure ejected K^+ simultaneously from two intraretinal micropipettes to simulate the two light-evoked b-wave $[K^+]_o$ increases. They found that the intraretinal voltage generated by the simultaneous ejections reached a minimal value at a location between the two ejection sites. During the b-wave response, however, the intraretinal voltage has a minimum value near the outer plexiform layer, i.e., at the site of the distal $[K^+]_o$ increase. Yanagida and Tomita (50) concluded that the b-wave cannot be generated solely by $[K^+]_o$ changes.

Our simulations suggest, however, that intraretinal b-wave profiles as well as the K^+ ejection profiles of Yanagida and Tomita (50) can both be generated according to the K^+ hypothesis. Simulation of the dual K^+ ejection experiment in our model system (Fig. 7*A*) yields intraretinal voltage profiles very similar to the experimental results. The intraretinal voltage reaches a minimum at a location midway between the two K^+ sources. Yet, when we simulate the $[K^+]_o$ changes that occur during the b-wave, a different pattern of intraretinal voltage is obtained. In this case (Fig. 7*B*), the minimum is located at 60% retinal depth, near the distal K^+ source.

The simulations demonstrate that differences in the locations, magnitudes, and time courses of the K^+ sources are of critical importance. Both the proximal and distal K^+ sources used in the b-wave simulation are located more distally than are the corresponding K^+ ejection sites used by Yanagida and Tomita (50) (in our simulation, 22–32% and 53–63% for the b-wave versus 24–26% and 47–49% for the K^+ ejections). Due partly to this difference in K^+ source location, the distal K^+ source contributes a greater percentage to the total intraretinal potential in the b-wave simulation than in the K^+ ejection simulation. Thus, we believe that Yanagida and Tomita's experiments do not reproduce the $[K^+]_o$ changes that occur during the b-wave accurately enough to function as a critical test of the K^+ hypothesis.

Magnitude of distal $[K^+]_o$ increase

A troubling aspect of the K^+ hypothesis is that the distal $[K^+]_o$ increases that have been measured in some experimental systems do not appear to be large enough to generate the b-wave currents of the distal retina. In our simulation of b-wave generation, we use a distal K^+ increase that is 62% as large as the proximal increase in peak amplitude. This produces b-wave current source-density and intraretinal potential profiles that resemble the experimental data. This distal $[K^+]_o$ increase is larger than those measured in some experimental preparations. However, Kline et al. (21) and Dick and Miller (11) have observed distal increases that are greater than 50% the amplitude of the proximal one.

The distal $[K^+]_o$ increase, as measured by K^+-selective micropipettes, is often elusive. Some investigators fail to observe it at all (41, 49). Others do measure a distal increase, but only occasionally. Karwoski and Proenza (20), for instance, have recently reported a distal $[K^+]_o$ increase in the frog, but see it in only 60% of their penetrations. Even when a distal increase is seen, its amplitude can vary greatly from penetration to penetration.

A possible clue to this puzzling behavior comes from an observation of Kline, Ripps,

and Dowling (21) (J. E. Dowling, personal communication). They were able to record distal $[K^+]_o$ increases only as they advanced their K^+-selective micropipette into the retina from the vitreal surface. If they first advanced the micropipette past the neural retina and into the pigment epithelium and then measured $[K^+]_o$ on withdrawal of the pipette, they failed to see a distal increase. This suggests that retinal damage caused by the micropipette itself may be compromising $[K^+]_o$ measurements.

How might this come about? A dead space will be created around the tip of the ion-selective micropipette, especially as it is withdrawn from the retina. Within this dead space, the effective volume fraction of extracellular space will be increased and K^+ sources (depolarizing neurons) will be destroyed. Thus $[K^+]_o$ measured at the center of a dead space will not reflect the true value of $[K^+]_o$ in normal retinal tissue but rather will reflect the $[K^+]_o$ level produced as K^+ diffuses from the undamaged tissue into the middle of the damaged region. The larger the region of damaged tissue, the smaller will be the apparent value of $[K^+]_o$ change measured by the micropipette.

We have modeled the conditions created by micropipette damage in retinal tissue in order to assess their effects on $[K^+]_o$ levels in the distal retina. In our model, the region of damage is described by a cylindrical volume of diameter d and length d. $[K^+]_o$ is measured at the center of this region. To measure the distal $[K^+]_o$ increase, this damaged region is centered at 58% depth, at the middle of the distal K^+ source. Within the simulated region of damage, the volume fraction of extracellular space is increased from 7% (the value in undamaged tissue) to 100%. The tortuosity factor is reduced from 1.8 to 1.0, increasing D_K (apparent) to $2 \cdot 10^{-5}$ cm^2/s.

Figure 10 illustrates the effect of tissue damage on $[K^+]_o$ levels at 58% depth. When the diameter of damage (d) is set to 0, the normal distal $[K^+]_o$ increase is obtained. As d is increased, the $[K^+]_o$ level at the center of the damaged region is reduced. At the same time, the latency to the peak of the increase is lengthened, as expected from the delay introduced by K^+ diffusion to the middle of the damaged region. When the diameter of damage is small (<7.5 μm), $[K^+]_o$ is reduced little, but as d is increased, the reduction in $[K^+]_o$ becomes significant. For d values equal to 7.5, 12.5, and 20 μm, the peak amplitude of the $[K^+]_o$ increase is reduced to 91, 66, and 28% the normal value.

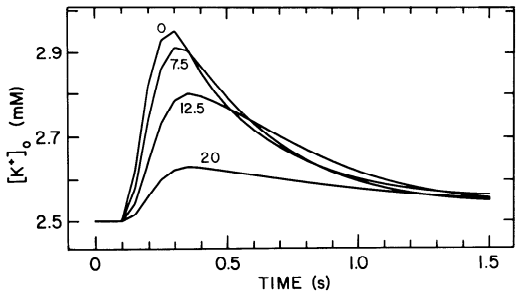

FIG. 10. Distal $[K^+]_o$ increase at the middle of a simulated region of retinal damage. Damaged region is a cylindrical volume of diameter and length d centered at 58% depth. The diameter of the damaged region (in micrometers) is given next to each trace. The 0 trace represents $[K^+]_o$ in an undamaged retina. As d is increased, the amplitude of $[K^+]_o$ is reduced and its latency to peak is lengthened.

The reduction of measured $[K^+]_o$ by retinal damage is due largely to the increase in volume fraction created by the damage. The magnitude of this reduction is critically dependent on the value of the volume fraction (α) of the undamaged tissue surrounding the damaged region. For a damaged region 12.5 μm in diameter, for instance, the peak $[K^+]_o$ increase is reduced to 45% when α (undamaged tissue) = 0.023, 66% when α = 0.07, and 81% when α = 0.21.

The simulation illustrated in Fig. 10 suggests that if the region of damage produced by an ion-selective micropipette is small (<7.5 μm in diameter) measured $[K^+]_o$ levels will not be compromised seriously. However, for larger regions of damage, such as those that might be produced by first advancing and then withdrawing a micropipette, measured $[K^+]_o$ levels could seriously underestimate the true amplitude of the increase. We have chosen to model b-wave generation in our simulations using a relatively large distal $[K^+]_o$ increase for this reason.

Predictions of model

Our simulation of the K^+ hypothesis has led to a number of predictions. *1*) The location of the reversal point within the retina, where the b-wave potential shifts from a positive to

a negative response when referenced to the sclera, will vary with the magnitude of the extraretinal shunt resistance. The reversal point will shift proximally when the shunt resistance is reduced. *2*) Larger distal $[K^+]_o$ increases will be measured experimentally if greater care is taken to prevent retinal damage by K^+-selective micropipettes. Larger increases may also be recorded under conditions where the distal $[K^+]_o$ decrease is kept to a minimum. *3*) Using the experimental paradigm of Yanagida and Tomita (50), intraretinal K^+ ejections will generate voltage profiles that vary depending on the location of the ejection site. Dual K^+ ejections will generate an intraretinal voltage profile similar to that of the b-wave when ejection pipettes are positioned at the sites of the two light-evoked $[K^+]_o$ increases. *4*) K^+-mediated current efflux from the high-permeability Müller cell endfoot represents a secondary K^+ source. A small but significant light-evoked $[K^+]_o$ increase will occur in this region and should be measurable in the vitreous adjacent to the retina and in the optic fiber layer. *5*) Reduction or destruction of the large K^+ permeability of the Müller cell endfoot will result in a dramatic rearrangement of b-wave current flow. This will cause a large decrease in the amplitude of the transretinal b-wave response.

The means to selectively reduce endfoot K^+ permeability are not known at this time. Mechanical destruction (complete or vigorous draining of the vitreous) or anoxia are two possible candidates. The gradual decrease in b-wave amplitude seen in experimental preparations while neuronal responses remain intact may be due to deterioration of Müller cell endfoot permeability.

In conclusion, simulations in our model retina strongly support the K^+ hypothesis of b-wave generation. The time course of the b-wave and Müller cell responses generated by the model resemble those recorded experimentally. The distribution of current source-density and of intraretinal b-wave potential also match experimental findings. The predictions suggested by our simulations will provide further tests for the K^+ hypothesis.

APPENDIX

The most general form of the equations used to model the K^+ hypothesis require solution of the complete electrodiffusion problem since ion fluxes are composed of both electrical drift and diffusion components. We chose instead to decouple the electrical problem from the diffusion problem. This is justified, since we are only concerned with the distribution of ions over dimensions much greater than the Debye length (25). Thus, we proceed by first solving the diffusion problem for the distribution of $[K^+]_o$ and then solve the electrical problem for the distribution of potential and current.

The solution to the diffusion problem gives the change in $[K^+]_o$ as a function of retinal depth and time. The homogeneous equation of continuity is

$$\frac{d[K^+]_o}{dt} = D^* \frac{d^2[K^+]_o}{dz^2} - [K^+]_o\left(\frac{1}{\tau_p \alpha} + \frac{1}{\tau_a}\right) - \frac{G_{m,j}}{F\alpha_j}(\Delta V_j) \quad (5)$$

as described in the MODEL section of this paper.

Equation 5 is solved numerically using a predictor-corrector method based on the Crank-Nicolson procedure (Ref. 1, p. 85). Given a concentration specified at depth $(j)\Delta z$ and at time (i) Δt, the predictor calculates the concentration at the intermediate time point $(i + \frac{1}{2})\Delta t$. The corrector is then used to calculate the concentration at time point $(i + 1)\Delta t$.

The predictor is

$$\frac{2}{\Delta t}([K_o]_{i+\frac{1}{2},j} - [K_o]_{i,j}) - \frac{D_j^*}{(\Delta z)^2}\delta_z^2[K_o]_{i+\frac{1}{2},j} - [K_o]_{i,j}\left(\frac{1}{\tau_{p,j}\alpha_j} + \frac{1}{\tau_a}\right) - \frac{G_{m,j}}{F\alpha_j}\Delta V_{i,j} \quad (6a)$$

The corrector is

$$\frac{1}{\Delta t}([K_o]_{i+1,j} - [K_o]_{i,j}) = \frac{D_j^*}{2(\Delta z)^2}\delta_z^2([K_o]_{i+1,j} + [K_o]_{i,j}) - [K_o]_{i+\frac{1}{2},j}\left(\frac{1}{\tau_{p,j}\alpha_j} + \frac{1}{\tau_a}\right) - \frac{G_{m,j}}{F\alpha_j}\Delta V_{i+\frac{1}{2},j} \quad (6b)$$

where δ_z^2 is the central difference operator

$$\delta_z^2[K_o]_{i,j} \equiv [K_o]_{i,j+1} - 2[K_o]_{i,j} + [K_o]_{i,j-1}$$

Increases or decreases in $[K^+]_o$ in a given time interval due to a K^+ source or sink are included by incrementing or decrementing $[K^+]_j$ prior to computing the new value of $[K^+]_j$.

Equations 6a and *6b*, together with concentration increments or decrements due to a K^+ source or sink, relate the concentration profile at one point in time to the concentration profile after a time increment, Δt. We use the Thomas tridiagonal algorithm (5) to solve this set of equations for the new concentration profile.

Once a concentration profile at a particular time is known, we calculate the transmembrane Nernst potential (V) for each spatial increment j, and then solve for the mesh current, i_j (see the circuit diagram,

Fig. 2). We include a mesh current term, i_s, to describe the current flowing through the extraretinal shunt resistance, R_s.

The voltage distribution is found by writing the mesh equations for the circuit. The mesh current in interval j, i_j, is described by the following equation

$$V_j - V_{j+1} = -R_{e,j}i_s - R_{m,j}i_{j-1} + (R_{e,j} + R_{i,j} + R_{m,j} + R_{m,j+1})i_j - R_{m,j+1}i_{j+1}$$

The matrix of mesh equations has the form

$$\begin{bmatrix} -R_{e,1} & R_{L,1} & -R_{m,2} & & & & \\ -R_{e,2} & -R_{m,1} & R_{L,2} & -R_{m,3} & & 0 & \\ -R_{e,3} & & -R_{m,2} & R_{L,3} & -R_{m,4} & & \\ \vdots & & & \ddots & \ddots & \ddots & \\ & & 0 & & -R_{m,n-2} & R_{L,n-1} & -R_{m,n} \\ -R_{e,n-1} & & & & & -R_{m,n-1} & R_{L,n} \\ -R_{e,n} & & & & & & \\ R_s + \Sigma R_{e,j} & -R_{e,1} & -R_{e,2} & -R_{e,3} & \cdots & -R_{e,n-2} & -R_{e,n-1} & -R_{e,n} \end{bmatrix} \cdot \begin{bmatrix} i_s \\ i_1 \\ i_2 \\ \vdots \\ i_{n-2} \\ i_{n-1} \\ i_n \end{bmatrix} = \begin{bmatrix} V_1 - V_2 \\ V_2 - V_3 \\ V_3 - V_4 \\ \vdots \\ V_{n-1} - V_n \\ V_n - V_{n+1} \\ 0 \end{bmatrix} \quad (7)$$

where

$$R_{L,j} = R_{e,j} + R_{i,j} + R_{m,j} + R_{m,j+1}$$

Since the set of mesh equations differs from a tridiagonal set by the shunt current term, i_s, we split the set of equations, treating the shunt term as a current source and use a relaxation method to find an approximation to the solution. The iteration matrix is tridiagonal and can be solved by the Thomas algorithm.

We truncate our iteration procedure when

$$\left| \frac{(R_s + \Sigma R_{e,j})i_s}{\Sigma R_{e,j} i_j} - 1 \right| < 0.001$$

which indicates a close approximation to the solution of the last equation of the set in *equation 7*. The calculated mesh currents are then a close approximation to the solution of the complete problem.

Once the mesh currents are calculated, the distribution of potential in extracellular space or within the Müller cell is calculated by applying Ohm's law to find the voltages generated as the mesh currents flow through $R_{e,j}$ and $R_{i,j}$. The current source-density magnitude in interval j is calculated from the difference between mesh currents in adjacent intervals, that is, $i_j - i_{j+1}$.

ACKNOWLEDGMENTS

We are grateful to Peter H. Hartline for the generous loan of his computer system and to Peter H. Hartline, Ralph Zuckerman, and an anonymous reviewer for their valuable comments on the manuscript.

This research was supported by National Institutes of Health Grant EY 04077 and The Charles A. King Trust, Boston, to E. A. Newman and National Science Foundation Grants BNS 801539 and BNS 7824162 to P. H. Hartline.

Received 6 July 1982; accepted in final form 11 August 1983.

REFERENCES

1. AMES, W. F. *Numerical Methods for Partial Differential Equations.* New York: Barnes & Noble, 1969.
2. BAKER, P. F., BLAUSTEIN, M. P., KEYNES, R. D., MANIL, J., SHAW, T. I., AND STEINHARDT, R. A. The ouabain-sensitive fluxes of sodium and potassium in squid giant axons. *J. Physiol. London* 200: 459–496, 1969.
3. BRINDLEY, G. S. AND HAMASAKI, D. I. The properties and nature of the R-membrane of the frog's eye. *J. Physiol. London* 167: 599–606, 1963.
4. BROWN, K. T. AND WIESEL, T. N. Localization of origins of electroretinogram components by intraretinal recording in the intact cat eye. *J. Physiol. London* 158: 257–280, 1961.
5. CARNAHAN, B., LUTHER, H. A., AND WILKES, J. O. *Applied Numerical Methods.* New York: Wiley, 1969.
6. CASTELLUCCI, V. F. AND GOLDRING, S. Contribution to steady potential shifts of slow depolarization in cells presumed to be glia. *Electroencephalogr. Clin. Neurophysiol.* 28: 109–118, 1970.
7. COHEN, A. I. A possible cytological basis for the R-membrane in the vertebrate eye. *Nature London* 205: 1222–1223, 1965.
8. COHEN, M. W. The contribution by glial cells to surface recordings from the optic nerve of an amphibian. *J. Physiol. London* 210: 565–580, 1970.
9. CRANK, J. *The Mathematics of Diffusion.* New York: Oxford University Press, 1975.
10. DICK, E. AND MILLER, R. F. Light-evoked potassium activity in mudpuppy retina: its relationship to the b-wave of the electroretinogram. *Brain Res.* 154: 388–394, 1978.

11. DICK, E. AND MILLER, R. F. The electroretinogram: neural origins of extracellular K^+ activity changes related to ERG components. I. Amphibian (I-type) retinas. *J. Gen. Physiol.* In press.
12. FABER, D. S. *Analysis of Slow Transretinal Potentials in Response to Light* (Ph.D. Thesis). Buffalo: State University of New York, 1969.
13. FISHER, R. S., PEDLEY, T. A., AND PRINCE, D. A. The kinetics of potassium movement in normal cortex. *Brain Res.* 101: 223–237, 1976.
14. FUJIMOTO, M. AND TOMITA, T. Field potentials induced by injection of potassium ion into the frog retina: a test of current interpretations of the electroretinographic (ERG) b-wave. *Brain Res.* 204: 51–64, 1981.
15. HARNED, H. S. AND NUTTALL, R. L. The differential diffusion coefficient of potassium chloride in aqueous solutions. *J. Am. Chem. Soc.* 71: 1460–1463, 1949.
16. HASHIMOTO, Y., MURAKAMI, M., AND TOMITA, T. Localization of the ERG by aid of histological method. *Jpn. J. Physiol.* 11: 62–69, 1961.
17. KARWOSKI, C. J. AND PROENZA, L. M. Relationship between Müller cell responses, a local transretinal potential, and potassium flux. *J. Neurophysiol.* 40: 244–259, 1977.
18. KARWOSKI, C. J. AND PROENZA, L. M. Light-evoked changes in extracellular potassium concentration in mudpuppy retina. *Brain Res.* 142: 515–530, 1978.
19. KARWOSKI, C. J. AND PROENZA, L. M. Neurons, potassium, and glia in proximal retina of *Necturus*. *J. Gen. Physiol.* 75: 141–162, 1980.
20. KARWOSKI, C. J. AND PROENZA, L. M. Light-evoked K^+ increases in amphibian retina. *Invest. Ophthalmol.* 22, Suppl.: 281, 1982.
21. KLINE, R. P., RIPPS, H., AND DOWLING, J. E. The generation of b-wave currents in the skate retina. *Proc. Natl. Acad. Sci. USA* 75: 5727–5731, 1978.
22. KUFFLER, S. W. Neuroglial cells: physiological properties and a potassium mediated effect of neuronal activity on the glial membrane potential. *Proc. R. Soc. London Ser. B* 168: 1–21, 1967.
23. LUX, H. D. AND NEHER, E. The equilibration time course of K^+_o in cat cortex. *Exp. Brain Res.* 17: 190–205, 1973.
24. MATSUURA, T., MILLER, W. H., AND TOMITA, T. Cone-specific c-wave in the turtle retina. *Vision Res.* 18: 767–776, 1978.
25. MELCHER, J. R. *Continuum Electromechanics*. Cambridge, MA: MIT Press, 1981.
26. MILLER, R. F. AND DOWLING, J. E. Intracellular responses to the Müller (glial) cells of mudpuppy retina: their relation to b-wave of the electroretinogram. *J. Neurophysiol.* 33: 323–341, 1970.
27. MORI, S., MILLER, W. H., AND TOMITA, T. Müller cell function during spreading depression in frog retina. *Proc. Natl. Acad. Sci. USA* 73: 1351–1354, 1976.
28. MORI, S., MILLER, W. H., AND TOMITA, T. Microelectrode study of spreading depression (SD) in frog retina—Müller cell activity and K^+ during SD. *Jpn. J. Physiol.* 26: 219–233, 1976.
29. NEWMAN, E. A. b-Wave currents in the frog retina. *Vision Res.* 19: 227–234, 1979.
30. NEWMAN, E. A. Current source-density analysis of the b-wave of frog retina. *J. Neurophysiol.* 43: 1355–1366, 1980.
31. NEWMAN, E. A. Regional differences in retinal Müller cell membrane properties. *Soc. Neurosci. Abstr.* 7: 275, 1981.
32. NEWMAN, E. A. Retinal glial cell endfeet have high K^+ conductance. *Soc. Neurosci. Abstr.* 9: 807, 1983.
33. NEWMAN, E. A. AND LETTVIN, J. Y. Relation of the e-wave to ganglion cell activity and rod responses in the frog. *Vision Res.* 18: 1181–1188, 1978.
34. NEWMAN, E. A. AND ODETTE, L. L. Model of electroretinogram b-wave generation: testing the K^+ hypothesis. *Soc. Neurosci Abstr.* 8: 50, 1982.
35. NICHOLSON, C. Dynamics of the brain cell microenvironment. *Neurosci. Res. Prog. Bull.* 18: 177–322, 1980.
36. NICHOLSON, C. AND FREEMAN, J. A. Theory of current source-density analysis and determination of conductivity tensor for anuran cerebellum. *J. Neurophysiol.* 38: 356–368, 1975.
37. NICHOLSON, C. AND PHILLIPS, J. M. Ion diffusion modified by tortuosity and volume fraction in the extracellular microenvironment of the rat cerebellum. *J. Physiol. London* 321: 225–257, 1981.
38. NICHOLSON, C., PHILLIPS, J. M., AND GARDNER-MEDWIN, A. R. Diffusion from an iontophoretic point source in the brain: role of tortuosity and volume fraction. *Brain Res.* 169: 580–584, 1979.
39. OAKLEY, B., II. *Measurement of Light-Induced Transient Changes in Extracellular Potassium Ion Concentration in the Frog Retina* (Ph.D. Thesis). Ann Arbor: University of Michigan, 1975.
40. OAKLEY, B., II, FLAMING, D. G., AND BROWN, K. T. Effects of the rod receptor potential upon retinal extracellular potassium concentration. *J. Gen. Physiol.* 74: 713–737, 1979.
41. OAKLEY, B., II AND GREEN, D. G. Correlation of light-induced changes in retinal extracellular potassium concentration with c-wave of the electroretinogram. *J. Neurophysiol.* 39: 1117–1133, 1976.
42. PROENZA, L. M. AND FREEMAN, J. A. Light-evoked extracellular potentials of the *Necturus* retina: current source density analysis of the electroretinographic b-wave and the proximal negative response. *Soc. Neurosci. Abstr.* 5: 104, 1975.
43. RASMUSSEN, K.-E. A morphometric study of the Müller cell in rod and cone retinas with and without retinal vessels. *Exp. Eye Res.* 20: 151–166, 1975.
44. STEINBERG, R. H., OAKLEY, B., II, AND NIEMEYER, G. Light-evoked changes in K^+_o in the retina of the intact cat eye. *J. Neurophysiol.* 44: 897–921, 1980.
45. TOMITA, T. The electroretinogram, as analyzed by microelectrode studies. *Handbook of Sensory Physiology*. Berlin: Springer-Verlag, 1972, vol. VII, part 2, p. 635–665.
46. TOMITA, T., MURAKAMI, M., AND HASHIMOTO, Y. On the R-membrane of the frog's eye: its localization, and relation to the retinal action potential. *J. Gen. Physiol.* 43, Suppl. 6: 81–94, 1960.
47. TOMITA, T. AND TORIHAMA, T. Further study on the intraretinal action potentials and on the site of ERG generation. *Jpn. J. Physiol.* 6: 118–136, 1956.
48. TOMITA, T. AND YANAGIDA, T. Origins of the ERG waves. *Vision Res.* 21: 1703–1707, 1981.
49. VOGEL, D. A. *Potassium Release and ERG b-Wave Current Flow in the Frog Retina* (Ph.D. Thesis). Ann Arbor: University of Michigan, 1980.
50. YANAGIDA, T. AND TOMITA, T. Local potassium concentration changes in the retina and the electroretinographic (ERG) b-wave. *Brain Res.* 237: 479–483, 1982.